EVS28
KINTEX, Korea, May 3-6, 2015

Characterising Li-ion battery degradation through the identification of perturbations in electrochemical battery models

Kotub Uddin[1], Surak Perera[2], Widanalage D. Widanage[1], James Marco[1]

[1] *WMG, International Digital Laboratory, The University of Warwick, Coventry, CV4 7AL, UK;*
k.uddin@warwick.ac.uk; dhammika.widanalage@warwick.ac.uk; james.marco@warwick.ac.uk
[2] *Maplesoft Europe Ltd, Broers Building, 21 JJ Thompson Avenue, Cambridge, CB3 OFA, UK;*
sperera@maplesoft.com

Abstract

Lithium ion batteries undergo complex electrochemical and mechanical degradation. This complexity is pronounced in applications such as electric vehicles where highly demanding cycles of operation and varying environmental conditions lead to non-trivial interactions of ageing stress factors. This work presents the framework for an ageing diagnostic tool based on identifying the physical parameters of a fundamental electrochemistry-based battery model from non-invasive voltage/current cycling tests. Exploiting the embedded symbolic manipulation tool and global optimiser in MapleSim, computational cost is reduced, significantly facilitating rapid optimisation. The diagnostic tool is used to study the degradation of a 3Ah LiC_6/$LiNiCoAlO_2$ battery stored at 45℃ at 50% State of Charge for 202 days; the results agree with expected battery degradation.

Keywords: Li-ion battery; ageing; EV; modelling; parameterisation

1 Introduction

Since the commercialisation of Lithium-ion batteries, significant improvements in energy density and power capability has made lithium ion batteries a preferred solution for low carbon mobility [1]. The change in behaviour of Li-ion batteries over a vehicle lifetime can have a significant effect on vehicle performance and lifetime [2, 3]. Exploring the causes of battery ageing and developing mitigation strategies to avoid premature ageing is, therefore of paramount importance to vehicle manufacturers.

The study of battery ageing is complicated as many factors from environmental conditions to vehicle utilization interact to generate different ageing effects [4]. Battery degradation is accelerated with frequency of cycling, large state of charge swings (ΔSOC), large current magnitudes, elevated temperatures, and elevated voltage exposure, among other factors [2]. The resulting physical degradation [4] can broadly manifest itself in three ways that a systems engineer is interested in: capacity fade which can affect the range of the vehicle; increases in the internal resistance or impedance of the cell known as power fade which can limit the power or decrease the efficiency of the vehicle; and ultimately may even lead to failure.

In this work we apply sustainable, non-destructive techniques to quantify the degradation associated with ageing accelerants. Although the data provides a valuation for capacity fade and power fade, detailed interpretation, diagnosis and prognosis of degradation and failure requires mathematical models to be developed. To this end, we develop an electrochemistry based battery ageing model which extends the work of Doyle Fuller and Newman [5], that combines

concentrated solution kinetics, mass conservation, charge conservation, and transport and conduction in porous media. To investigate battery degradation perturbative terms are introduced into the model parameters. Using a non-linear fitting algorithm, the evolution of these perturbations are then derived by minimising square error with aged, non-invasive voltage/current cycling tests and matched with phenomenological degradation models identified and reported in the literature.

Offline parameter identification of battery models using cycling data is widely employed for equivalent circuit battery models where a set of *n* parallel resistor–capacitor pairs are connected to each other in series [3, 6]. Parameters of higher fidelity models such as the Single Particle (SP) model with various dynamic and thermal extensions have also been identified using various identification methods [7]. Santhanagopalan et. al. [8] for example used the Levenberg–Marquardt optimization algorithm to identify a subset of five parameters for both the Pseudo 2D Porous electrode model (P2D) and SP models using constant charge and discharge cycles. An important contribution to parameter identification was made by Forman et. al. [9] who identified the full set of parameters (88 scalars and function control points) of the P2D model using a genetic algorithm using PHEV vehicle drive cycle data. To the best of the authors' knowledge such identification methods, however, have not been employed within the context of studying battery degradation, in particular, diagnostics.

A key achievement in this work was minimising the computational resources required for optimising a large parameter set. The Symbolic Manipulator embedded within Maple is used to simplify the system of equations generated for the model during compilation leading to an improvement in computational effort required to solve the system of equations.

The remainder of this article is organised as follows. Section 2 describes the mathematical formulation of the P2D model. In section 3 the model partners are discussed. The optimisation scheme is presented in section 4. In section 5 we present some diagnostic results of aged cells. Section 6 summarizes and concludes the paper.

2 Model formulation

The 1D lithium ion cell depicted in Figure 1 consists of three domains: negative electrode (in this work LiC_6), separator (in this work polyethylene) and positive electrode (in this work $LiNiCoAlO_2$) sandwiched between current collectors and immersed in an electrolyte solution. During discharge, lithium ions that occupy interstitial sites in the LiC_6 electrode diffuse to the surface where they react (de-intercalate) and transfer from a solid into a liquid phase. The ions then diffuse and migrate through the electrolyte solution via the separator to the positive electrode where they react (intercalate) and occupy an interstitial site at the metal oxide material.

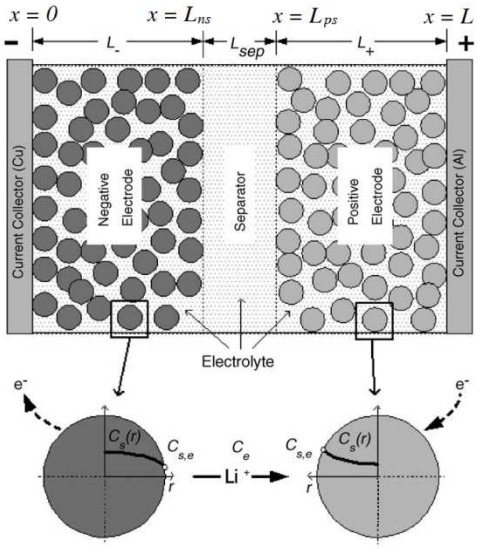

Figure 1: Schematic of the Pseudo 2D electrochemical cell model comprising of 1D (x-directional) liquid phase dynamics and 1D (r-direction) solid diffusional dynamics.

The rate of intercalation and de-intercalation reactions that occur at the electrode and electrolyte interface is assumed to follow a Butler-Volmer relation:

$$\begin{aligned} j &= Fk(c_e)^{\alpha_a}(c_s^{max} \\ &- c_{s,e})^{\alpha_a}(c_{s,e})^{\alpha_c}\left\{exp\left[\frac{\alpha_a F}{RT}\left(\eta - \frac{R_{film}}{a_s}j\right)\right]\right. \\ &\left. - exp\left[\frac{-\alpha_c F}{RT}\left(\eta - \frac{R_{film}}{a_s}j\right)\right]\right\} \end{aligned} \quad (1)$$

where j is the current density across the electrode/electrolyte interface, F is Faraday's constant, k is a rate constant of lithium

interaction/de-interaction, c stands for the volume-averaged lithium concentration, with subscripts e, s and s,e referring to the concentration in the electrolyte, solid and solid/electrolyte interface, respectively. The anodic and cathodic transfer coefficients of electrode reactions are denoted by α_a and α_c, R is the universal gas constant and T the absolute temperature. The local surface over-potential η is defined as

$$\eta = \phi_s - \phi_e - U \tag{2}$$

where ϕ is the volume-averaged potential in a phase and U is the open circuit potential. The term R_{film} represents a finite film resistance on the electrode surface. The specific interfacial area of the porous electrode a_s is given by

$$a_s = \frac{3}{r}\varepsilon_s = \frac{3}{r}(1 - \varepsilon_e - \varepsilon_f). \tag{3}$$

where ε_s, ε_e and ε_f represent the porosity (volume fraction) of the solid active material, electrolyte and current conductive fillers respectively, in the electrode regions. The diffusion of Lithium ions within the electrolyte is governed by Fick's law of linear diffusion combined with the intercalation current density (j) transferring Li-ions between the solution and solid [10]:

$$\frac{\partial(\varepsilon_e c_e)}{\partial t} = \nabla \cdot \left(D_e^{eff} \nabla c_e\right) - \frac{i_e \nabla t_+^0}{F} + \frac{1 - t_+^0}{F} a_s j \tag{4}$$

where i_e is current density in the electrolyte, t_+ is the transference number – which in reference to the velocity of the solvent is assumed to be constant due to the lack of data in literature – and D_e^{eff} is the effective diffusivity coefficient inside the porous electrode corrected via the Bruggeman relation

$$D_e^{eff} = D_e {\varepsilon_e}^{3/2}. \tag{5}$$

The latter is a correction for tortuosity that arises from porous electrode theory where the solid porous active material and a liquid electrolyte are treated as superimposed continua without regard to microstructure.

After the free lithium become intercalated lithium on the surface of the particles, the interacted lithium diffuse into the bulk of the active material solid electrolyte particles. This diffusion occurs at every point in the anode and cathode and can be modelled using Fick's second law – a spherical, radially symmetric diffusion law – as follows:

$$\frac{\partial(\varepsilon_s c_s)}{\partial t} = \frac{D_s}{r^2}\frac{\partial}{\partial r}\left(r^2 \frac{\partial c_s}{\partial r}\right). \tag{6}$$

where D_s is the diffusivity coefficient of the solid phase and r is the radius of an electrode. Using Duhamel superposition to re-write the right hand side of Eq. (6) as a Volterra integral and subsequently solving the right hand side, Doyle et. al. [5] showed that this term is proportional to current density j in the electrode. Gu and Wang [11] in their work replaced the right hand side of Eq. (6) by a first-order differential equation describing the conservation of lithium in the solid phase,

$$\frac{\partial(\varepsilon_s c_s)}{\partial t} = \frac{-a_s j_{int}}{F}. \tag{7}$$

Conservation of charge in the solid phase is given by Ohm's law

$$\nabla.\left(\sigma_s^{eff} \nabla \phi_s\right) = a_s j \tag{8}$$

where the effective conductivity of the solid phase is related to the conductivity of the active material through the porosity of the solid:

$$\sigma_s^{eff} = \sigma_s {\varepsilon_s}^{3/2}. \tag{9}$$

The conservation of charge in the electrolyte phase is given by

$$\nabla \cdot \left(\kappa_e^{eff} \phi_e\right) + \nabla \cdot \left[\frac{2R\kappa_e^{eff}}{F}(t_+^0 - 1)\left(1 + \frac{d\ln(f_\pm)}{d\ln(c_e)}\right)\nabla \phi_e\right] = -a_s j, \tag{10}$$

where the effective ionic conductivity is given by the Bruggeman correction for the tortuosity $\kappa_e^{eff} = \kappa_e {\varepsilon_e}^{3/2}$ and the mean molar activity coefficient of the electrolyte is taken to be a constant [10].

The open circuit potential U in Eq. (2) is a function of the lithium concentration of the solid phase at the solid electrode/electrolyte interface $c_{s,e}$, i.e., $U_+ = U_+\left(\theta_+\left(c_{s,e,+}\right)\right)$ and $U_- = U_-\left(\theta_-\left(c_{s,e,-}\right)\right)$ where

$$\theta_+ = \frac{c_{s,e,+}}{c_{s,+}^{max}} \quad \text{and} \quad \theta_- = \frac{c_{s,e,-}}{c_{s,-}^{max}} \tag{11}$$

and the battery state of charge is defined by the ratio θ_+/θ_-.

The system described above has two independent variables, i.e., x and t, and five unknown variables, namely ϕ_e, ϕ_s, c_e, c_s and $c_{s,e}$, which are calculated by simultaneously solving equations (1), (4), (6), (8) and (10) with initial and boundary conditions listed below. The cell terminal voltage is defined by

$$V_{cell} = \phi_s(t,0) - \phi_s(t,L) - \frac{R_f}{A} I \qquad (12)$$

where A the electrode plate surface area and I is the cell current.

The initial conditions are:

$$c_s = c_{s,e} = c_s^0, \qquad c_e = c_e^0 \qquad (13)$$

The boundary conditions associated with the concentration of electrolyte are:

$$\left.\frac{\partial c_e}{\partial x}\right|_{x=0} = \left.\frac{\partial c_e}{\partial x}\right|_{x=L} = 0 \qquad (14)$$

To ensure continuity at the boundaries of the separator:

$$D_{e,n}^{eff} \left.\frac{\partial c_e}{\partial x}\right|_{x=L_{ns}^-} = D_{e,mem}^{eff} \left.\frac{\partial c_e}{\partial x}\right|_{x=L_{ns}^+} \qquad (15)$$

$$D_{e,mem}^{eff} \left.\frac{\partial c_e}{\partial x}\right|_{x=L_{ps}^-} = D_{e,p}^{eff} \left.\frac{\partial c_e}{\partial x}\right|_{x=L_{ps}^+} \qquad (16)$$

where the subscript mem refers to the membrane separator.

The boundary conditions for the potential of the solid phase are:

$$\left.\frac{\partial \phi_s}{\partial x}\right|_{x=L_{ns}^-} = \left.\frac{\partial \phi_s}{\partial x}\right|_{x=L_{ps}^+} = 0 \qquad (17)$$

$$-\sigma_{s,n}^{eff} \left.\frac{\partial \phi_s}{\partial x}\right|_{x=0} = \frac{-I}{S_n} = \sigma_{s,p}^{eff} \left.\frac{\partial \phi_s}{\partial x}\right|_{x=L} = \frac{I}{S_p} = i(t). \qquad (18)$$

The boundary conditions for the potential of the electrolyte phase are:

$$\kappa_{e,n}^{eff} \left.\frac{\partial \phi_e}{\partial x}\right|_{x=0} = \kappa_{e,p}^{eff} \left.\frac{\partial \phi_e}{\partial x}\right|_{x=L} = 0 \qquad (19)$$

$$\kappa_{e,n}^{eff} \left.\frac{\partial \phi_e}{\partial x}\right|_{x=L_{ns}^-} = \kappa_{e,mem}^{eff} \left.\frac{\partial \phi_e}{\partial x}\right|_{x=L_{ns}^+} \qquad (20)$$

$$\kappa_{e,mem}^{eff} \left.\frac{\partial \phi_e}{\partial x}\right|_{x=L_{ps}^-} = \kappa_{e,p}^{eff} \left.\frac{\partial \phi_e}{\partial x}\right|_{x=L_{ps}^+} \qquad (21)$$

3 Model parameters

There are a total of 57 scalar parameters listed in Table 1 of which 21 belong to the open circuit potentials U_+ and U_-. The positive electrode equilibrium potential function U_+ is identified from cell open circuit voltage measurements, assuming a known negative electrode (Li_xC_6) equilibrium potential function U_- from the literature. This leaves a remaining 36 parameters that require identification.

Table 1: Initial values that are taken from Refs. [8] (†), [12] (*) and [13] (‡) are indicated by corresponding symbols.

Parameter	Symbol	Initial value
Thickness of negative electrode	L_- $(10^{-4}\ cm)$	149.9
Thickness of positive electrode	L_+ $(10^{-4}\ cm)$	134.0
Thickness of separator	L_{sep} $(10^{-4}\ cm)$	25.0
Surface area of negative electrode,	A_- (cm^2)	428.4
Surface area of positive electrode	A_+ (cm^2)	389.61
Surface area of separator	A_{sep} (cm^2)	448.35
Modal radius of negative electrode particle	$R_{s,-}$ $(10^{-4}\ cm)$	10.7
Modal radius of positive electrode particle	$R_{s,+}$ $(10^{-4}\ cm)$	5.7
Active material volume fraction of negative electrode	$\varepsilon_{s,-}$	0.3
Active material volume fraction of positive electrode	$\varepsilon_{s,+}$	0.3
Electrolyte phase volume fraction of negative electrode	$\varepsilon_{e,-}$	0.595
Electrolyte phase volume fraction of positive electrode	$\varepsilon_{e,+}$	0.63
Volume fraction of separator in liquid phase	$\varepsilon_{e,sep}$	0.5
Volume fraction of inactive material in negative electrode	$\varepsilon_{f,-}$	0.105
Volume fraction of inactive material in positive electrode	$\varepsilon_{f,+}$	0.07
Maximum li-	$c_{s,-}^{max}$	†30.6

concentration in negative electrode	$(10^{-3} mol\ cm^{-3})$	
Maximum li-concentration in positive electrode	$c_{s,+}^{max}$ $(10^{-3} mol\ cm^{-3})$	†51.6
Average electrolyte concentration,	$c_{e,0}$ $(10^{-3} mol\ cm^{-3})$	*1.2
Stoichiometry of negative electrode at 0% SoC,	$x_{-,0}$	*0.126
Stoichiometry of positive electrode at 0% SoC	$x_{+,0}$	*0.936
Stoichiometry of negative electrode at 100% SoC	$x_{-,100}$	*0.676
Stoichiometry of positive electrode at 100% SoC	$x_{+,100}$	*0.442
Diffusion coefficient of negative electrode in solid phase	$D_{s,-}$ $(10^{-12} cm^2 s^{-1})$	1.14
Diffusion coefficient of positive electrode in solid phase	$D_{s,+}$ $(10^{-12} cm^2 s^{-1})$	*3.7
Diffusion coefficient in liquid phase	D_e $(10^{-6} cm^2 s^{-1})$	*2.6
Conductivity of negative electrode in solid phase	$\sigma_{s,-}$ $(S\ cm^{-1})$	*1.0
Conductivity of positive electrode in solid phase	$\sigma_{s,+}$ $(S\ cm^{-1})$	†1.0
Charge transfer coefficient in negative electrode	$k_{e,-}$ $(10^{-6} cm^{2.5} mol^{-0.5} s^{-1})$	‡1.764
Charge transfer coefficient in positive electrode	$k_{e,+}$ $(10^{-6} cm^{2.5} mol^{-0.5} s^{-1})$	‡3.626
Anodic charge transfer coefficient	α_a	0.5
Cathodic charge transfer coefficient	α_c	0.5
Li transference number	t_+^0	0.36
Electrolyte activity coefficient	$f_\pm$	1.0
Bruggeman porosity exponent	p	1.5
Resistance of film layers (including SEI)	R_{film} (Ωcm^2)	0.0
Resistivity of the current collector	R_f (Ωcm^2)	20.1
Negative electrode potential, U_- coefficients	$b_1^- - b_{11}^-$	
Positive electrode potential, U_+, coefficients	$b_1^+ - b_{10}^+$	

where the electrode potentials are defined in the form:

$$U_- = b_1^- + b_2^- x_- + b_3^- {x_-}^{0.5} + b_4^- {x_-}^{-1} + b_5^- {x_-}^{1.5} + b_6^- exp[b_7^-(b_8^- - x_-)] + b_9^- exp[b_{10}^-(x_- - b_{11}^-)] \quad (22)$$

$$U_+ = b_1^+ + b_2^+ x_+ + b_3^+ {x_+}^2 + b_4^+ {x_+}^3 + b_5^+ {x_+}^4 + b_6^+ {x_+}^5 + b_7^+ {x_+}^6 + b_8^+ exp\left[b_9^+ {x_+}^{b_{10}^+}\right] \quad (23)$$

and the stoichiometry is defined by:

$$x_- = x_{-,0} + (x_{-,100} - x_{-,0})\frac{SoC}{100} \quad (24)$$

$$x_+ = x_{+,0} + (x_{+,100} - x_{+,0})\frac{SoC}{100} \quad (25)$$

Of these 36 parameters, stoichiometry of both electrodes at 100% and 0% SoC, anodic and cathodic charge transfer coefficients, the electrolyte activity co-efficient and the Bruggemen coefficient are assumed to be constant with values compatible with those found in the literature. Only a subset of the remaining 28 parameters will change depending on the exact mode of ageing.

A comprehensive summary of expected parameter modifications resulting from battery degradation is beyond the scope of this paper; readers are referred to a forthcoming publication by the authors on *"Characterising Li-ion battery degradation through the identification of model parameters."* For general reviews of battery degradation the reviews by Vetter et. al. [4] and Barré [14] et. al. are recommended.

4 Model parameterisation

The electrochemical model equations given in Section 2 are solved using finite differences in MapleSim. To achieve fast simulation times which subsequently facilitate non-linear parameter fittings the symbolic manipulator embedded within MapleSim, during compilation, removes redundant equations and generates a highly optimised model code in C. Because the battery model is stiff, a robust numerical solver is required; in this work the Rosenbrock solver is employed.

For a cell "aged" by one or more of the identified stress factors, a current cycling profile and corresponding voltage response at a given cell age is used to estimate the model parameters (or a subset of them). The trace of the optimised parameters with age allows cell degradation to be characterised and consequently the nature of the phenomenological degradation mechanism.

The optimum parameters for a given data set are obtained by minimising a quadratic error cost function (equation 26). In Eq. (26) v_e is the experimentally measured voltage, v_m is the model voltage and γ is the vector of parameters to be optimised.

$$\begin{aligned} Minimise\ F(\gamma) = \frac{1}{2}\sum_{t=0}^{t_{max}} [v_e(t) \\ - v_m(t,\gamma)]^2 \\ subject\ to\ \gamma_i \geq 0 \end{aligned} \quad (26)$$

The bounded nonlinear optimisation problem Eq. (26) is iteratively minimised using a differential evolution algorithm (`differvol`) within MapleSim's Global Optimisation package. In multi-objective, stochastic problems with non-linear, non-differentiable objective functions and multiple possible local minima, such as the problem in this work, this evolutionary algorithm is a well-established method for deriving approximate solutions [15]. As the minimisation routine is iterative the values listed in Table 1 are used as initial guesses to initiate the optimisation algorithm and terminates if the maximum number of iterations is reached or the variation over each successively optimised parameters is below a predefined tolerance.

5 Results and discussion

Let us consider the degradation of the 3.03Ah $LiNiCoAlO_2$ 18650 cell stored at 45℃ at 50% SoC for 202 days. At such elevated temperatures the most notable cause of degradation is electrolyte decomposition reactions at the negative electrode/electrolyte boundary which consume lithium ions – resulting in capacity fade – subsequently forming a solid electrolyte interface (SEI) layer on the negative electrode surface. The SEI then acts as an impediment to ionic diffusion leading to power fade. The parameters of interest therefore, are: maximum number of accessible lithium sites ($c_{s,-}^{max}$) which will govern capacity fade; film resistance (R_{film}) which will reflect power fade; and radius of negative electrode particle ($R_{s,-}$) which will also contribute to power fade through the increased solid diffusion path length.

The potential U_- of the graphite (Li_xC_6) negative electrode is assumed to initially follow the empirical correlation from Ref. [16]. The positive electrode potential (U_+) is derived by subtracting U_- from the cell's open circuit voltage and then fitting to equation (23) using non-linear least squares:

$$\begin{aligned} U_+ \\ = 7.3203 - 42.6905x_+ + 211.1859{x_+}^2 \\ - 504.6774{x_+}^3 + 614.6070{x_+}^4 \\ - 367.1214{x_+}^5 + 84.1478{x_+}^6 \\ - 0.0016exp[-10.8867{x_+}^{-10.4676}] \end{aligned} \quad (27)$$

Using U_- from Ref. [16] and U_+ as defined in equation (27) the parameter values listed in Table 1 are fine-tuned against the initial (age 0 days) 1C discharge curve. This new "fine-tuned" parameter set forms the base set of parameters from which ageing causes deviations.

The aged cells are characterised approximately every 9 to10 weeks. The P2D model is fitted to the 1C discharge curves optimising for $c_{s,-}^{max}$, R_{film} and $R_{s,-}$. The model fitting results are shown in Figure 2.

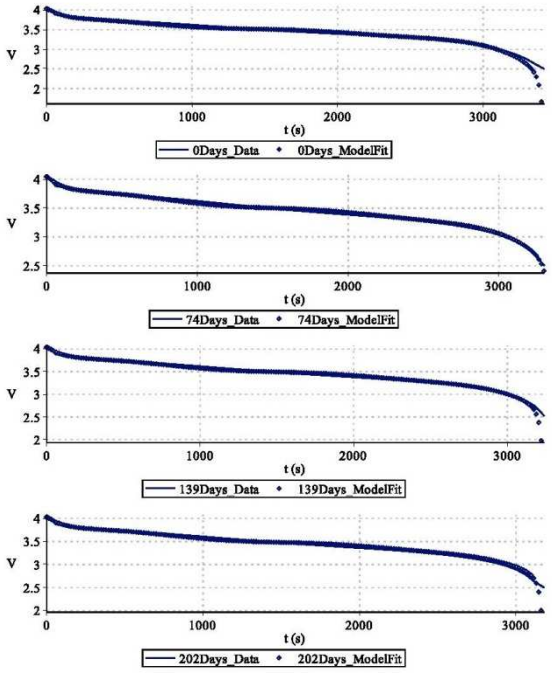

Figure 2: Voltage profiles under 1C discharge of NCA 3.03Ah cells stored at 45℃ at 50% SoC. The solid lines show experiment results; the markers indicate fitted results.

Variations of $c_{s,-}^{max}$, R_{film} and $R_{s,-}$ as a function of age are depicted in Figure 3 to Figure 5, respectively. As expected, there is a rise in resistance and fall in capacity.

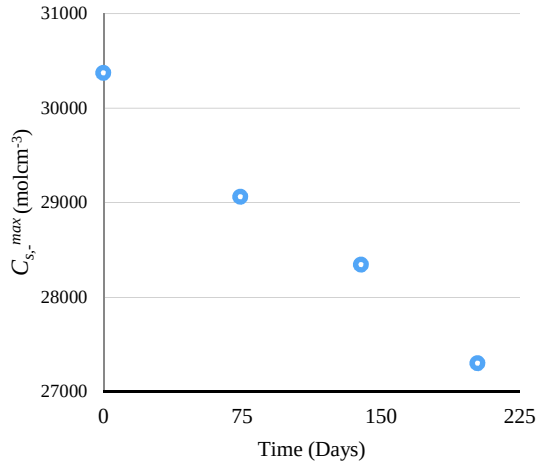

Figure 3: Changes in maximum lithium concentration of negative electrode ($c_{s,-}^{max}$) as a function of calendar age.

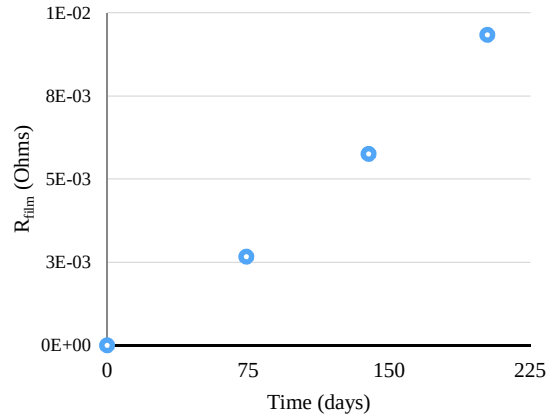

Figure 4: Changes in film resistance (R_{film}) as a function of calendar age.

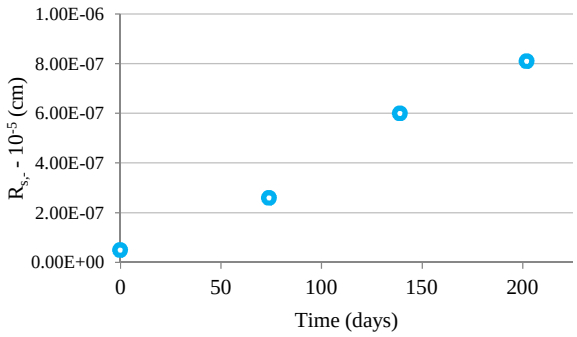

Figure 5: Changes in negative electrode particle radius ($R_{s,-}$) as a function of calendar age.

The rise of film resistance is consistent with results derived from Electrochemical Impedance Spectroscopy tests. Capacity fade predictions estimated from variations in $c_{s,-}^{max}$ are also consistent with direct analysis of the experimental results shown in Figure 1.

6 Conclusion

The framework for a battery ageing diagnostics technique employing non-invasive voltage/current cycling tests was presented. The work employs a differential evolution optimisation algorithm to iteratively identify the parameters of the P2D battery model by minimising the sum of square errors between predicted voltage and experimental measurements for a 1C discharge curve. After identifying a set of "fine-tuned parameters" corresponding to a new cell, subsequent fittings are made on aged cells to track parameter changes. It is shown that these parameter changes can highlight intrinsic battery degradation. —As an example, degradation of a 3.03Ah $LiC_6/LiNiCoAlO_2$ battery stored at 45℃ at 50% SoC for 202 days is studied. Given that under these conditions growth of the SEI layer is the dominant ageing mechanism, variations of $c_{s,-}^{max}$, R_{film} and $R_{s,-}$ as a function of calendar age was traced. These parameters were found to evolve, under these conditions, in agreement with trends identified in the literature.

The procedure employed in this work allows for a set of parameter values for the P2D model to be identified quickly and noninvasively. Model compilation, initialisation and initial simulation take approximately ten minutes; subsequent runs for a single parameter set is considerably less than a second. Thus, to optimise a subset of three parameters can take less than 20 seconds – significantly quicker than the 63 seconds for a single run reported in Ref. [9].

It is expected that unique identifiability of parameters for this model will be limited. In an ensuing paper therefore, the authors will provide an analysis of parameter sensitivity and model validation. While the ability to accurately match voltage curves is expected not change, how the data is interpreted to insinuate intrinsic battery degradation mechanisms may be effected.

Acknowledgments

The authors thank Dr Gael Chouchelamane for gathering the ageing data and Dr Christopher Lyness and Dr Michael Lain for fruitful discussions. The research presented within this paper is supported by MapleSoft Europe Ltd. as well as Innovate UK through the WMG Centre High Value Manufacturing (HVM) Catapult in collaboration with Jaguar Land Rover.

References

[1] J.-M. Tarascon, M. Armand, Issues and challenges facing rechargeable lithium batteries, Nature, 414 (2001) 359-367.

[2] K. Smith, M. Earleywine, E. Wood, J. Neubauer, A. Pesaran, Comparison of Plug-In Hybrid Electric Vehicle Battery Life Across Geographies and Drive Cycles, SAE Technical Paper, (2012) 01-0666.

[3] P.A. Uddin K, Lyness C, Taylor N, Marco J, Acausal Li-ion battery pack model for automotive applications, Energies, 7 (2014) 5675-5700.

[4] J. Vetter, P. Novak, M. Wagner, C. Veit, K.-C. Möller, J. Besenhard, M. Winter, M. Wohlfahrt-Mehrens, C. Vogler, A. Hammouche, Ageing mechanisms in lithium-ion batteries, Journal of power sources, 147 (2005) 269-281.

[5] M. Doyle, T.F. Fuller, J. Newman, Modeling of galvanostatic charge and discharge of the lithium/polymer/insertion cell, Journal of the Electrochemical Society, 140 (1993) 1526-1533.

[6] Y. Hu, S. Yurkovich, Y. Guezennec, B. Yurkovich, Electro-thermal battery model identification for automotive applications, Journal of Power Sources, 196 (2011) 449-457.

[7] A.P. Schmidt, M. Bitzer, Á.W. Imre, L. Guzzella, Experiment-driven electrochemical modeling and systematic parameterization for a lithium-ion battery cell, Journal of Power Sources, 195 (2010) 5071-5080.

[8] S. Santhanagopalan, Q. Guo, R.E. White, Parameter estimation and model discrimination for a lithium-ion cell, Journal of the Electrochemical Society, 154 (2007) A198-A206.

[9] J.C. Forman, S.J. Moura, J.L. Stein, H.K. Fathy, Genetic identification and fisher identifiability analysis of the Doyle–Fuller–Newman model from experimental cycling of a LiFePO< sub> 4</sub> cell, Journal of Power Sources, 210 (2012) 263-275.

[10] G. Ning, R.E. White, B.N. Popov, A generalized cycle life model of rechargeable Li-ion batteries, Electrochimica acta, 51 (2006) 2012-2022.

[11] C. Speltino, D. Domenico, G. Fiengo, A. Stefanopoulou, Experimental identification and validation of an electrochemical model of a lithium-ion battery, in: Proceedings of the American Control Conference, 2009.

[12] K. Smith, C.-Y. Wang, Solid-state diffusion limitations on pulse operation of a lithium ion cell for hybrid electric vehicles, Journal of Power Sources, 161 (2006) 628-639.

[13] Y. Ye, Y. Shi, N. Cai, J. Lee, X. He, Electro-thermal modeling and experimental validation for lithium ion battery, Journal of Power Sources, 199 (2012) 227-238.

[14] A. Barré, B. Deguilhem, S. Grolleau, M. Gérard, F. Suard, D. Riu, A review on lithium-ion battery ageing mechanisms and estimations for automotive applications, Journal of Power Sources, 241 (2013) 680-689.

[15] R. Storn, K. Price, Differential evolution–a simple and efficient heuristic for global optimization over continuous spaces, Journal of global optimization, 11 (1997) 341-359.

[16] M. Doyle, Y. Fuentes, Computer simulations of a lithium-ion polymer battery and implications for higher capacity next-generation battery designs, Journal of The Electrochemical Society, 150 (2003) A706-A713.

Authors

Dr Kotub Uddin holds a doctorate in Theoretical Physics. After graduating he joined the Department of Research at Jaguar Land Rover as a Senior Research Engineer working on design

optimisation and control. He later transferred to the Hybrids Research team working on mathematical modelling of electrochemical systems for energy storage and automotive battery design. Kotub is currently employed as a Senior Research Fellow at The University of Warwick researching energy storage systems and applications to low carbon transport.

Surak Perera holds an MEng in Aerospace Engineering from the University of Southampton. After graduating he worked as an applications engineer at Adept Scientific. He is currently an Applications Engineer at MapleSoft Europe Ltd where he specialises in systems level modelling of complex multi-domain systems within automotive, aerospace and energy industries.

Dr Dhammika Widanage was awarded a Ph.D. in 2008 for research done at the Stochastic and Complex Systems Laboratory Group from the University of Warwick. Prior to joining WMG he was a Post-doctoral Researcher and Post-doctoral Research Fellow at the Department of Electric Engineering and Energy Technology and the Department of Fundamental Electricity and Instrumentation at the Vrije Universiteit Brussel, Belgium. Dhammika is a member of the Institute of Electrical and Electronic Engineers (IEEE).

Dr James Marco is a Chartered Engineer and a member of the Institution of Engineering and Technology (IET). After graduating with an Engineering Doctorate, James worked for several years within the automotive industry on a number of different projects including those involving Ford (North America and Europe), Jaguar Cars, Land Rover and Daimler Chrysler. He is currently employed as an Associate Professor in Vehicle Electrification and Energy Storage at Warwick Manufacturing Group, University of Warwick.